Journal of
Materials Chemistry A

Accepted Manuscript

This is an *Accepted Manuscript*, which has been through the RSC Publishing peer review process and has been accepted for publication.

Accepted Manuscripts are published online shortly after acceptance, which is prior to technical editing, formatting and proof reading. This free service from RSC Publishing allows authors to make their results available to the community, in citable form, before publication of the edited article. This *Accepted Manuscript* will be replaced by the edited and formatted *Advance Article* as soon as this is available.

To cite this manuscript please use its permanent Digital Object Identifier (DOI®), which is identical for all formats of publication.

More information about *Accepted Manuscripts* can be found in the **Information for Authors**.

Please note that technical editing may introduce minor changes to the text and/or graphics contained in the manuscript submitted by the author(s) which may alter content, and that the standard **Terms & Conditions** and the **ethical guidelines** that apply to the journal are still applicable. In no event shall the RSC be held responsible for any errors or omissions in these *Accepted Manuscript* manuscripts or any consequences arising from the use of any information contained in them.

Simulations of Hydrogen Sorption in *rht*-MOF-1: Identifying the Binding Sites Through Explicit Polarization and Quantum Rotation Calculations

Tony Pham,[†,§] Katherine A. Forrest,[†,§] Adam Hogan,[†] Keith McLaughlin,[†]
Jonathan L. Belof,[‡] Juergen Eckert,[†] Brian Space*[,†]
[†]*Department of Chemistry, University of South Florida,*
4202 E. Fowler Ave., CHE205, Tampa, FL 33620-5250
[‡]*Lawrence Livermore National Laboratory,*
7000 East Ave., Livermore, CA 94550

ABSTRACT: Grand canonical Monte Carlo (GCMC) simulations of hydrogen sorption were performed in *rht*-MOF-1, a metal-organic framework (MOF) that consists of isophthalate groups joined by copper paddlewheel clusters and Cu_3O trimers through tetrazolate moeities. This is a charged *rht*-MOF that contains extra-framework nitrate counterions within the material. For the simulations performed herein, excellent agreement with experiment was achieved for the simulated hydrogen sorption isotherms and calculated isosteric heat of adsorption, Q_{st}, values only when using a polarizable potential. Thermodynamic agreement is demonstrated *via* comparing to experimental isotherms and binding sites are revealed by combining simulation and inelastic neutron scattering (INS) data. Simulations involving explicit many-body polarization interactions assisted in the determination of the binding sites in *rht*-MOF-1 through the distribution of the induced dipoles that led to strong adsorbate interactions. Four distinct hydrogen sorption sites were determined from the polarization distribution: the nitrate ions located in the corners of the truncated tetrahedral cages, the Cu^{2+} ions of the paddlewheels that project into the truncated tetrahedral and truncated octahedral cages (Cu1 ions), the Cu^{2+} ions of the Cu_3O trimers (Cu3 ions), and the sides of the paddlewheels in the cuboctahedral cage. The simulations revealed that the initial sorption sites for hydrogen in *rht*-MOF-1 are the nitrate ions; this site corresponds to the high initial Q_{st} value for hydrogen (9.5 $kJmol^{-1}$) in the MOF. The radial distribution functions, g(r), about the Cu^{2+} ions at various loadings revealed that the Cu1 ions are the preferred open-metal sorption sites for hydrogen at low loading, while the Cu3 ions become occupied at higher loadings. The validation of the aforementioned sorption sites in *rht*-MOF-1 was confirmed by calculating the two-dimensional quantum rotational levels about each site and comparing the levels to the transitions that were observed in the experimental INS spectra for hydrogen in the compound. For each binding site, the rotational transitions from $j = 0$ to $j = 1$ were in good agreement to certain transitions that were observed in the INS spectra. From these calculations, the assignment of the peaks in the INS spectra for hydrogen in *rht*-MOF-1 has been made.

I. INTRODUCTION

Molecular hydrogen has been recognized by many scientists as an alternative fuel source because it is clean, abundant, and has a high energy content per weight of fuel. Indeed, the combustion of hydrogen in an engine releases no greenhouse gases and generates approximately 120.7 kJ/g of energy, the highest of any known fuel.[1] Although hydrogen is a promising alternative to replace existing petroleum-based gasoline and diesel fuels, it tends to interact weakly with its environment, thus making the transport of neat hydrogen rather difficult.[2] In addition, the successful commercialization of hydrogen-powered vehicles depends on the development of safe, efficient, and economical on-board hydrogen storage systems.[3] The ultimate U.S. Department of Energy (DOE) target for an on-board hydrogen storage system is 0.075 kg/kg or 0.070 kg/L at ambient temperatures and high pressures.[4] Further, the fueling of hydrogen should be completely reversible, and the recharging process must be completed within minutes.

Metal-organic frameworks (MOFs) are an emerging class of crystalline porous materials that have been demonstrated to be promising for applications in hydrogen storage.[3,5–7] These materials consist of metal-ion clusters coordinated to organic ligands in a self-assembly process, resulting in a porous three-dimensional periodic structure.[8] MOFs have the ability to densely store hydrogen molecules into small areas through a physisorption process. They have also been shown to display high affinity for hydrogen with reversible sorption. This makes MOFs advantageous over competing materials for hydrogen storage, such as activated carbons,[9] zeolites,[10] and metal hydrides.[11] MOFs are highly tunable as a number of different structures can be synthesized by changing the metal-ion cluster and/or ligand.[12,13] Indeed, a number of MOFs with different pore sizes, topologies, and chemical functionalities have been synthesized within the past two decades.

The *rht*-MOF platform is a highly successful class of MOFs in the world of porous materials.[14–31] These MOFs are synthesized from metal ions that are coordinated to a C_3 symmetric ligand with three coplanar isophthalate moieties. Each isophthalate group is linked to metal ions to form a square paddlewheel, $[M_2(O_2CR)_4]$, cluster. A total of 24 isophthalate groups are connected by 12 paddlewheel clusters to form a cuboctahedron. In essence, *rht*-MOFs are characterized by linking a C_3 symmetric ligand with 24 edges of a cuboctahedron. It is for this reason that these MOFs are also called the 3,24-connected MOFs. Further, the overall structure of *rht*-MOFs contains three distinct cages: cuboctahedron, truncated tetrahedron, and truncated octahedron. *rht*-MOFs are a promising platform of MOFs because they contain open-metal sites, have high surface area, and have tunable pore sizes. They have been shown to display high uptake for a variety of energy-related gases, including hydrogen. A number of *rht*-MOFs have been synthesized by simply changing the size and functionality of the ligand.

The synthesis of *rht*-MOFs was pioneered by Eddaoudi and co-workers, with the first *rht*-MOF being synthesized in 2008.[14] This MOF, denoted *rht*-MOF-1, was synthesized by a solvothermal reaction of 5-tetrazolylisophthalic acid

Journal of Materials Chemistry A Accepted Manuscript

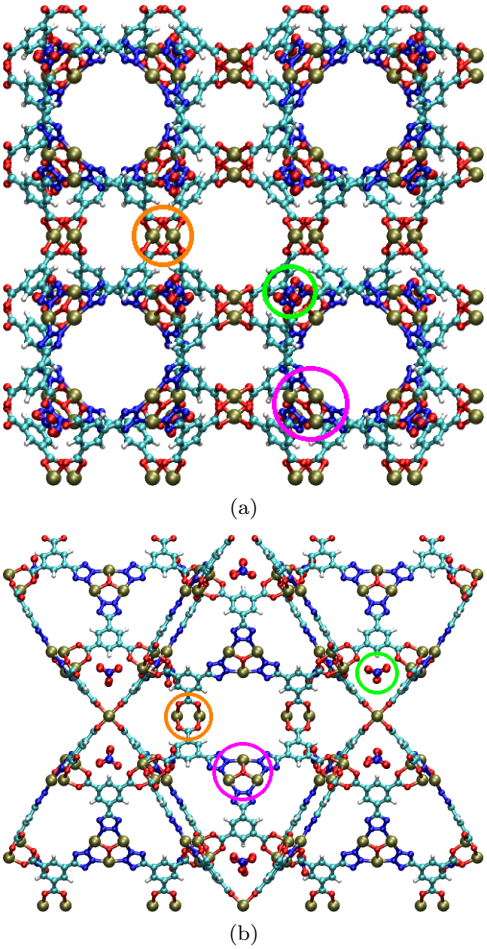

FIG. 1: **(a)** The $a/b/c$ view and **(b)** the view of the 45° angle between two axes of the unit cell of *rht*-MOF-1. The nitrate counterions, the copper paddlewheel clusters, and the Cu_3O trimers are indicated by the orange, magenta, and green circles, respectively. Atom colors: C = cyan, H = white, N = blue, O = red, Cu = tan.

(H_3TZI) with Cu^{2+} ions. *rht*-MOF-1 is characterized by trigonal Cu_3O trimers that are linked to these TZI ligands; the isophthalate groups of the ligand are then coordinated to Cu^{2+} ions to form the copper paddlewheel clusters (Figure 1). The MOF also contains nitrate counterions to balance the charge of the cationic framework. *rht*-MOF-1 is a MOF that has a large BET surface area of 2847 m^2g^{-1} (Langmuir surface area of 3223 m^2g^{-1}), a pore volume of 1.01 cm^3g^{-1}, and a porosity of 75 %. In addition, experimental hydrogen sorption measurements on the material have shown that *rht*-MOF-1 is capable of sorbing 2.4 wt % at 77 K and 1.0 atm, where wt % is defined as: [(Mass of H_2)/(Mass of MOF + Mass of H_2)] × 100 %. This MOF also displays a high isosteric heat of adsorption, Q_{st}, for hydrogen, with a value of approximately 9.5 $kJmol^{-1}$ at initial loading. Note, a hydrogen binding energy within the range of 15 to 30 $kJmol^{-1}$ has been proposed for room temperature hydrogen storage in porous materials.[32,33]

Methods such as grand canonical Monte Carlo (GCMC) simulations and inelastic neutron scattering (INS) can provide insights into the mechanism of hydrogen sorption in MOFs. GCMC simulation have been shown to be useful for identifying the favorable sorption sites in a MOF.[34] In addition, experimental observables such as sorption isotherms and the Q_{st} values can be generated using this method; these quantities are often compared to the corresponding experimental data. Outstanding agreement with experiment engenders confidence in a variety of molecular level predictions. INS studies of the hindered rotational transitions of hydrogen molecules sorbed in a MOF can be utilized to determine the hydrogen binding affinity at various sites in the framework.[25,35] The INS spectra for hydrogen in a MOF contains a significant amount of information, as each transition observed in the INS spectra corresponds to a specific binding site in the MOF. Moreover, the barriers of rotation imparted to the sorbed hydrogen molecule by the MOF as well as the intensity of each transition can provide insights into the hydrogen binding affinity about each site.

In this work, we use GCMC methods to investigate hydrogen sorption in *rht*-MOF-1. *rht*-MOF-1 is different from most other *rht*-MOFs (and other types of MOFs, in general) because it contains two types of open-metal Cu^{2+} ion sites through the copper paddlewheels and the Cu_3O trimers, and has extra-framework nitrate counterions that serves as potential sorption sites. These moieties contribute towards a highly charged/polar structure; thus, explicit polarization is expected to be extremely important for the simulations of gas sorption in this compound. Hence, the simulations performed herein included many-body polarization interactions as it was essential to incorporate such interactions in the simulations of hydrogen sorption in *rht*-MOF-1. These types of interactions have been shown to be important for the modeling of gas sorption in other charged/polar MOFs.[2,36–39] If many-body polarization was not included, the simulations would inaccurately capture the interaction between the adsorbate molecules and the open-metal sites and also underestimate experimental measurements.

Although initial hydrogen sorption simulation studies in *rht*-MOF-1 were performed by Babarao *et al.*, these simulations neglected the inclusion of induced dipole interactions.[40] As a result, their simulations undersorbed the experimental results across most of the pressure range and did not capture the sorption of hydrogen onto the open-metal sites. It is also noteworthy that the reported simulated hydrogen sorption isotherms at 77 K were inflated due to the lack of quantum corrections. Quantum mechanical effects have been shown to be important for hydrogen at this temperature due to its low molecular mass.[41,42] Thus, it is inaccurate to treat hydrogen in a classical manner under these conditions. In contrast, our simulations include quantum corrections *via* Feynman-Hibbs.[43]

Further, experimental INS studies were performed for hydrogen in *rht*-MOF-1 and the spectra revealed a number of transitions that correspond to a particular sorption site in the MOF.[25] Although some predictions of the sorption sites in the MOF have been made based on the observed transitions, the calculation of the quantum dynamics can verify these predictions, and thus, the assignments of the transitions in the INS spectra can accurately be achieved. In this work, we performed two-dimensional quantum rotation calculations for hydrogen about various sorption sites in *rht*-MOF-1 that were determined using the polarization distribution. Similar types of calculations have been performed for hydrogen sorption in MOFs in previous work.[44–47] The calculated rotational transitions are compared to those that were obtained from the INS studies. It will be shown that, for each hydrogen sorption site considered in *rht*-MOF-1, the calculated rotational level for the $j = 0$ to $j = 1$ transition corresponds to a specific peak within the INS spectra. As a result, a comprehensive interpetration of the INS spectra for hydro-

Journal of Materials Chemistry A Accepted Manuscript

gen in *rht*-MOF-1 can be obtained based on our calculations.

II. METHODS

A. Simulation Parameters

The potential energy of *rht*-MOF-1 is a function of repulsion/dispersion parameters, atomic point partial charges, and atomic point polarizabilities that are localized on the nuclear center of all atoms of the framework. Repulsion/dispersion interactions were modeled using the Lennard-Jones 12-6 potential, and these parameters for all MOF atoms were taken from the universal force field (UFF).[48] Although there are many van der Waals force fields that are available, the Lennard-Jones parameters from UFF were widely used in MOF–adsorbate studies performed earlier.[2,36,37,40,49–57] It is important to note that the UFF parameters are not completely transferable; however, they have been shown produce good results in certain systems (e.g., the MOF studied herein). The partial charges for the atoms in *rht*-MOF-1 were determined from electronic structure calculations on several fragments that were taken from the crystal structure of the MOF. More details of these calculations can be found in the Supporting Information. The polarizabilites for all light atoms were taken from van Duijnen *et al.*,[58] while the polarizability for Cu^{2+} was determined in previous work on PCN-61,[36] and used herein. The parameters for the MOF potential can be found in the Supporting Information. It should be noted that the polarizable force field used in this work is highly transferable and has already been shown produce excellent results in other charged/polar MOFs.[2,36,37]

Note, there are three chemically distinct Cu^{2+} ions in *rht*-MOF-1; they are denoted Cu1, Cu2, and Cu3 (Figure 2). The Cu1 and Cu2 ions are part of the copper paddlewheel clusters, while the Cu3 ion is part of the Cu_3O trimer unit that links the TZI ligands together. In addition, the Cu1 ion faces toward the center of the linker and projects into the truncated tetrahedral and truncated octahedral cages, while the Cu2 ion faces away from the center of the linker and projects into the cuboctahedral cages.

Simulations of hydrogen sorption in *rht*-MOF-1 were performed using a five-site polarizable hydrogen potential that was developed previously.[59] This hydrogen potential contain explicit parameters for repulsion/dispersion, stationary electrostatics, and induced-dipole interactions. This model was shown to reproduce bulk hydrogen data, especially at high densities,[59] and describe the proper sorption behavior in charged/polar MOFs that contain open-metal sites.[36,37] The interaction energy between the MOF and the hydrogen molecules was represented by the sum of the Lennard-Jones potential energy, the electrostatic energy as calculated by Ewald summation,[60] and the many-body polarization energy as calculated by the Thole-Applequist polarization model (explained in the Supporting Information).[61–64] Feynman-Hibbs quantum corrections[43] were implemented in this work to correct for the energetically dominant van der Waals interactions at low temperatures.

All simulations were performed using GCMC methods in a rigid single unit cell of *rht*-MOF-1. More details of the GCMC simulations can be found in the Supporting Information. Further, the simulations were performed with all nitrate ions held fixed in the corners of the truncated tetrahedral cages. This is the equilibrium location of the nitrate ions as determined from molecular dynamics (MD) simulations at low temperatures (see Supporting Information). Additional MD simulations revealed that the nitrate ions do not move from their equilibrium location even with the hydrogen molecules present in the MOF at low temperatures (see Supporting Information).

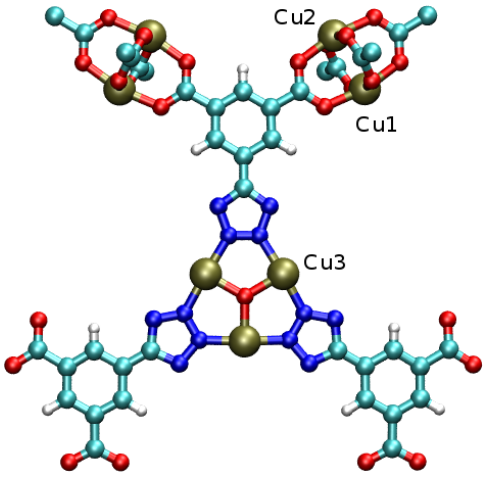

FIG. 2: The ligand, copper paddlewheel, and Cu_3O trimer units in *rht*-MOF-1. The labeling of the Cu1, Cu2, and Cu3 ions are also depicted. Atom colors: C = cyan, H = white, N = blue, O = red, Cu = tan.

B. Quantum Rotation Calculations

The two-dimensional quantum rotational levels for a hydrogen molecule about each site considered in *rht*-MOF-1 were calculated by diagonalizing the rotor Hamiltonian in the spherical harmonic basis, using methods reported previously,[45] which takes the following form:

$$\hat{H} = B\mathbf{j}^2 + V(\theta,\phi) \quad (1)$$

where B is the rotational constant for molecular hydrogen (equal to approximately 85.35 K[65]), $\mathbf{j}^2$ is the angular momentum operator, and $V(\theta,\phi)$ is the potential energy surface for the rotation of the hydrogen molecule with its center-of-mass held fixed within the MOF–H_2 system. Each matrix element, $\langle Y_{lm}|V(\theta,\phi)|Y_{lm}\rangle$, was constructed using Gauss-Legendre quadrature[66] with a basis set consisting of $\pm m$ functions.[67] The potential was generated over a 16 × 16 quadrature grid. The kinetic energy term, $j(j+1)$, was then added to the diagonal elements. The matrix was diagonalized using the LAPACK linear algebra package,[68] yielding the rotational energy eigenvalues and the eigenvector coefficients. All two-dimensional rotational levels were calculated with $j = 7$, leading to 64 basis functions. Note, including additional basis functions did not significantly alter the results. All calculations were performed using the Massively Parallel Monte Carlo (MPMC) code, an open-source code that is currently available for download on Google Code.[69]

III. RESULTS AND DISCUSSION

Figure 3(a) shows the simulated hydrogen sorption isotherm for the polarizable hydrogen potential in *rht*-MOF-

Journal of Materials Chemistry A Accepted Manuscript

1 at 77 K and 87 K compared to the corresponding experimental data (data points estimated from reference 14). It can be seen that excellent agreement with experiment is achieved at both temperatures using the polar model across the entire low-pressure range. The experimental hydrogen uptakes in *rht*-MOF-1 at 77 K and 87 K at 1.0 atm are 2.4 wt % and 1.7 wt %, respectively, and this agrees well with the calculations performed herein at those state points. Note, the error bars at each state point for the simulated plots are small (less than ± 0.02 wt %), and therefore, have been omitted for clarity.

It is important to emphasize that the simulated hydrogen sorption isotherms shown in Figure 3(a) can only be produced using a polarizable potential for the MOF and the hydrogen molecules. Models that neglect explicit many-body polarization effects are not sufficient to match the experimental hydrogen sorption isotherms in *rht*-MOF-1 due to the highly charged and polar environment of the framework. Indeed, control simulations using a hydrogen potential that contains only van der Waals interaction,[70] and two models that include only van der Waals and charge-quadrupole interactions[59,71] revealed that the simulated hydrogen sorption isotherms for these potentials undersorbed the experimental data by at least 22% over the entire pressure range considered at 77 K and 87 K (see Supporting Information).

Figure 3(b) shows the GCMC-calculated Q_{st} values for the polarizable hydrogen potential in *rht*-MOF-1 compared to the Q_{st} values that were derived experimentally (also estimated from reference 14). The former was determined using a statistical mechanical expression that involves the fluctuation of the number of particles and the total potential energy (see Supporting Information),[72] while the latter was determined by applying the Clausius–Clapeyron equation[73] to the experimental hydrogen sorption isotherms at 77 K and 87 K. The experimental initial Q_{st} value for hydrogen in *rht*-MOF-1 was calculated to be 9.5 kJmol^{-1}. Although this value is high, there are other MOFs that have higher initial Q_{st} values for hydrogen (e.g., Mg-MOF-74).[7,46,74–81] The experimental Q_{st} values decrease to approximately 4.75 kJmol^{-1} at 1.6 wt %. The Q_{st} values that were produced from simulation using the polar model in *rht*-MOF-1 were found to be in good agreement with experiment across all loadings. The simulated initial Q_{st} value for hydrogen was calculated to be 8.9 kJmol^{-1}, which is comparable to the experimental value at this loading. Any difference in the experimental and simulated Q_{st} values across the considered loading range might be attributed to the difference in methodology in computing the Q_{st} values for the respective techniques and associated uncertainities. As stated above, the experimental Q_{st} values are determined through empirical fitting of the experimental hydrogen sorption isotherms while the simulated Q_{st} values are obtained directly from GCMC simulation. Nonetheless, the close agreement between experiment and simulation is striking. As with the simulated hydrogen sorption isotherms, the Q_{st} plot shown in Figure 3(b) was only generated using the polarizable potential employed in this work. The Q_{st} values that were produced by the aforementioned nonpolarizable models severely underestimated the experimental Q_{st} values for all hydrogen uptakes (see Supporting Information).

Note, the initial hydrogen Q_{st} value for *rht*-MOF-1 surpasses most other MOFs that contain copper paddlewheel clusters.[7] For instance, previous studies have shown that the initial Q_{st} value for hydrogen in HKUST-1,[82] a prototypal MOF containing copper paddlewheels linked by 1,3,5-benzenetricarboxylate ligands, ranges from 6.0 to 7.0 kJmol^{-1}.[83–88] Similar values can be seen for other MOFs that contain these copper paddlewheels units.[17,37,89] Thus, this range for the Q_{st} value appears to be the appropriate energetics associated with the binding of the hydrogen molecules onto the Cu^{2+} ions of the copper paddlewheels. An initial Q_{st} value of 9.5 kJmol^{-1} for hydrogen in *rht*-MOF-1 is much greater than the values that are typically observed for sorption onto the copper paddlewheels; thus, we predict that this value must be attributed to the sorption of hydrogen onto a different type of moiety in the framework. This functionality must have a stronger interaction with the hydrogen molecules than the Cu^{2+} ions of the copper paddlewheels.

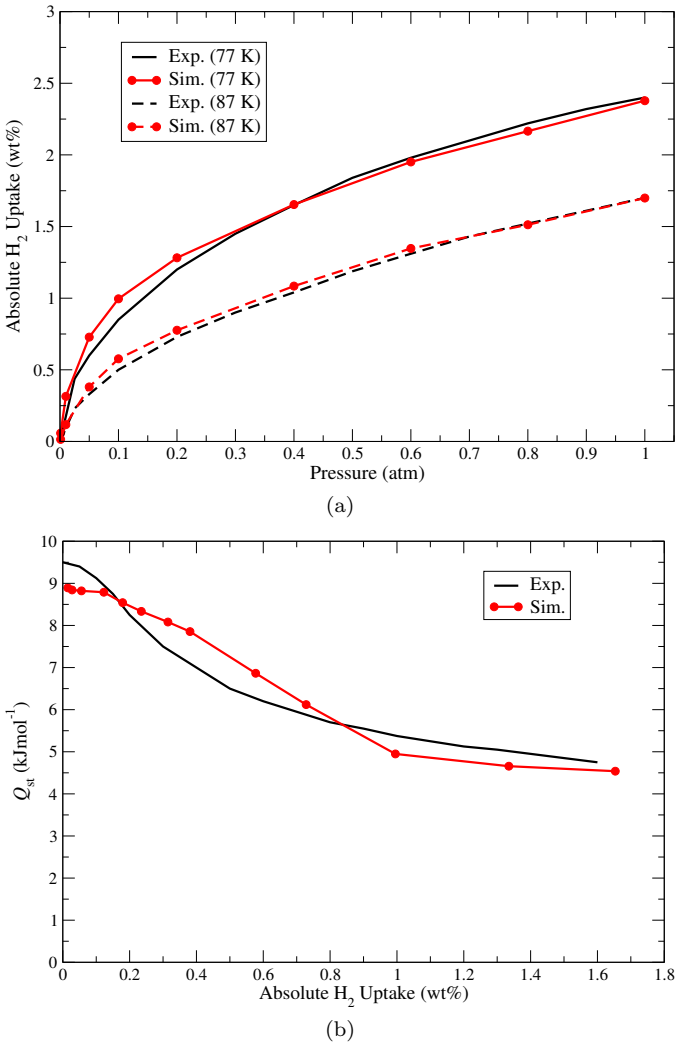

FIG. 3: **(a)** Low-pressure (up to 1.0 atm) absolute hydrogen sorption isotherms in *rht*-MOF-1 at 77 K (solid) and 87 K (dashed) for experiment (black) and simulation (red). **(b)** Isosteric heats of adsorption, Q_{st}, for hydrogen in *rht*-MOF-1 plotted against hydrogen uptakes for experiment (black) and simulation (red).

Examination of the Monte Carlo simulation history for hydrogen sorption in *rht*-MOF-1 at very low loading (77 K and 0.001 atm) revealed that the majority of hydrogen molecules are in the region of the nitrate ions that are located the corners of the truncated tetrahedral cage. In addition, examination of the three-dimensional histograms showing the most frequent sites of occupancy at this loading reveals that the majority of hydrogen molecules are sorbed to the nitrate ions

Journal of Materials Chemistry A Accepted Manuscript

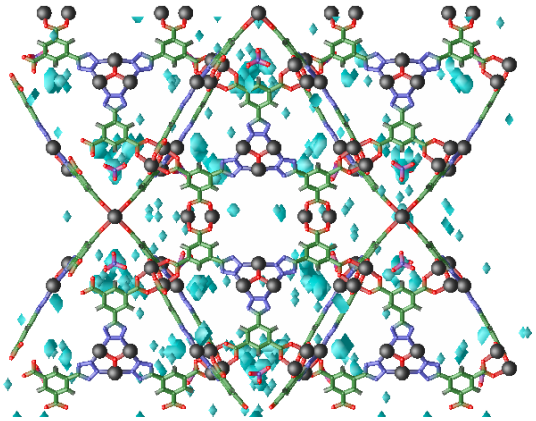

FIG. 4: The three–dimensional histogram in *rht*-MOF-1 showing the most frequent sites of occupancy (cyan) for hydrogen sorption at 77 K and 0.001 atm.

(Figure 4). Thus, the high initial Q_{st} value for hydrogen in *rht*-MOF-1 is attributed to the interaction between the hydrogen molecules and the nitrate ions. A molecular illustration (captured from the simulations) depicting this interaction is shown in Figure 5. Indeed, the uncoordinated nitrate ions are charged particles that increase the electrostatic field within the framework and they are more preferred for hydrogen sorption than the open-metal sites. This was verified by performing simulated annealing calculations for a single hydrogen molecule in *rht*-MOF-1 to identify the global minimum. This observation is consistent with previous findings that charged MOFs that contain extra-framework counterions have increased binding affinity towards hydrogen.[90]

The radial distribution functions, g(r), for the center-of-mass of the sorbed hydrogen molecules about all three types of Cu^{2+} ions in *rht*-MOF-1 at 77 K and two different pressures (0.01 atm and 1.0 atm) are shown in Figure 6. Note, the radial distribution functions shown herein are normalized to a total magnitude of unity over the distance examined. The g(r) results reveal that a large peak can be seen about the Cu1 ions at a distance of 2.5 Å at 0.01 atm. This radial distribution peak corresponds to the sorption of hydrogen molecules onto the Cu1 ions of the paddlewheels with a Cu^{2+}–H_2 distance of about 2.5 Å. The large magnitude of this peak at 0.01 atm signifies that this site is heavily populated with hydrogen molecules at low loading. At 1.0 atm, this peak for the Cu1 ion is reduced, which indicates that sorption onto the Cu1 ions is less prominent at this pressure. This is because the Cu1 ion sites are already filled at lower loadings, thus causing the hydrogen molecules to sorb to other regions in the MOF at higher pressures. Note, the Cu^{2+}–H_2 distance observed for *rht*-MOF-1 in this work is comparable to the corresponding distance that was observed in HKUST-1 through neutron powder diffraction and *ab initio* simulation studies.[44,91] In addition, analogous 2.5 Å radial distribution peaks of similar magnitudes can be seen about the favorable Cu^{2+} ion for simulations of hydrogen sorption in other *rht*-MOFs.[36,37] It is important to note that the observed radial distribution peak at 2.5 Å about the Cu1 ion can only be produced for simulations of hydrogen sorption using a polarizable model. Simulations using nonpolar potentials do not capture the sorption of hydrogen molecules onto the Cu^{2+} ions of the paddlewheels. This is because the Cu^{2+} ions are highly charged/polar species; induced dipole effects are required for sorption onto these sites. Note, for sorption onto the Cu1 ion in *rht*-MOF-1, a binding energy

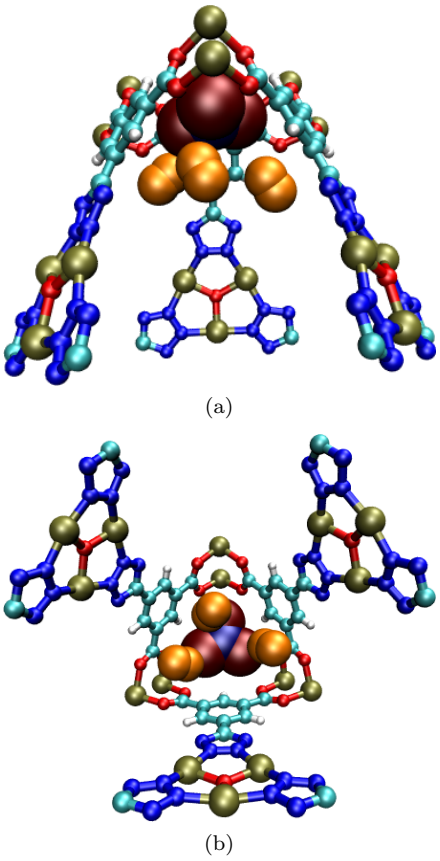

(a)

(b)

FIG. 5: Molecular illustration of the hydrogen binding site about the nitrate counterions in *rht*-MOF-1 as determined from simulation. **(a)** Side view **(b)** Down view. The adsorbate molecules are shown in orange. MOF atom colors: C = cyan, H = white, N = blue, O = red, Cu = tan. Nitrate atom colors: N = dark blue, O = maroon.

of approximately 6.5 kJmol^{-1} was calculated using canonical Monte Carlo (CMC); this value is within the range that is associated with sorption onto a single Cu^{2+} ion of a copper paddlewheel.

It can be observed from the g(r) results that there are only a few hydrogen molecules sorbed in the region of the Cu2 ions of the paddlewheels at both 0.01 atm and 1.0 atm in *rht*-MOF-1. Thus, even with the implementation of many-body polarization effects, the simulations capture only a small quantity of hydrogen molecules about the Cu2 ions. Indeed, for sorption onto the copper paddlewheels, the majority of hydrogen molecules sorb about the Cu1 ions. This is because the magnitude of the positive charge for the Cu2 ion is much less than that for the Cu1 ion as determined from electronic structure calculations on *rht*-MOF-1 (q_{Cu1} = 1.56 e^-, q_{Cu2} = 1.07 e^-, see Supporting Information). As stated earlier in the text, the two Cu^{2+} ions that are part of the paddlewheels in *rht*-MOFs are chemically distinct as both of these ions project into different regions in the MOF structure. It was demonstrated in previous theoretical studies that one of the Cu^{2+} ions of the paddlewheel has a higher charge magnitude relative to the other in *rht*-MOFs.[36,37] The charge distribution about the copper paddlewheels is dependent on the type of functionality on the organic linker. In *rht*-MOF-1, the linker contains nitrogen atoms on the tetrazolate group that are proximal to the Cu1 ions. The presence of these electronegative nitrogen atoms causes the Cu1 ion to exhibit a higher positive charge compared to the Cu2 ion. As a re-

Journal of Materials Chemistry A Accepted Manuscript

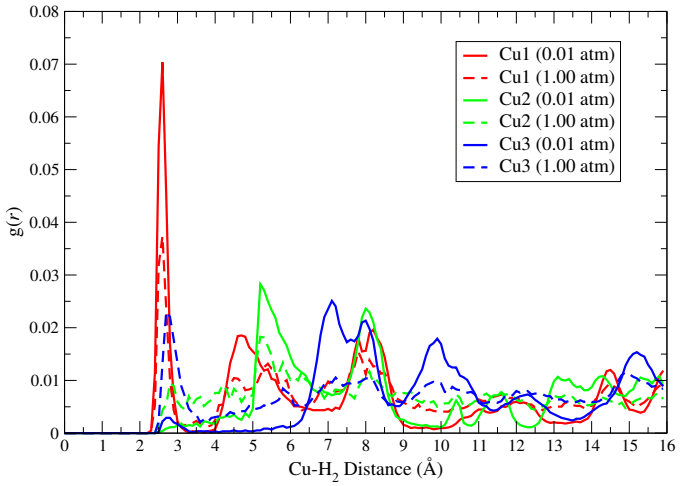

FIG. 6: Radial distribution functions, g(r), about the Cu1 ions (red), Cu2 ions (green), and Cu3 ions (blue) in *rht*-MOF-1 at 77 K and pressures of 0.01 atm (solid) and 1.0 atm (dashed).

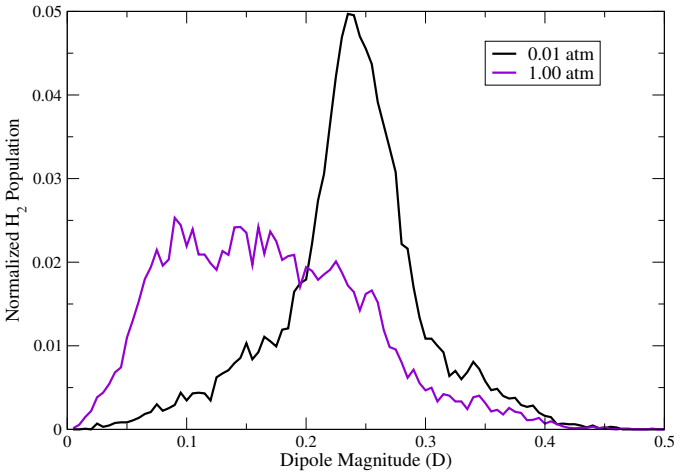

FIG. 7: Normalized hydrogen dipole distribution at 77 K and pressures of 0.01 atm (black) and 1.0 atm (violet) in *rht*-MOF-1.

sult, the Cu1 ion is more electron deficient, thus becoming the preferred sorption site for the hydrogen molecules about the copper paddlewheels.

rht-MOF-1 is different from most other *rht*-MOFs because it contains another type of open-metal Cu^{2+} ion in the structure; it is denoted as the Cu3 ion in this study. This Cu^{2+} ion is part of the Cu_3O trimer unit that links the TZI ligands together. The g(r) of the hydrogen molecules about the Cu3 ions shows that there are a small number of adsorbate molecules in the region of these ions at low loading. This is indicated by the small peak that was observed about this ion at a distance of approximately 2.7 Å at 0.01 atm. Thus, at low loading, the Cu3 ions are not as favored for hydrogen sorption compared to the Cu1 ion. This can be attributed to the difference in the electrostatic parameters between the two Cu^{2+} ions as the Cu3 ions have a lower positive charge than the Cu1 ions ($q_{Cu1} = 1.56\ e^-$, $q_{Cu3} = 0.88\ e^-$, see Supporting Information). However, it can be seen that the radial distribution peak at 2.7 Å for the Cu3 ion increases in magnitude at 1.0 atm. This indicates that the Cu3 ions become occupied at higher loadings for hydrogen sorption in *rht*-MOF-1. Note, the slightly higher nearest-neighbor distance for the hydrogen molecules around the Cu3 ions relative to the Cu1 ions also indicates that the hydrogen molecules do not sorb closely to the Cu^{2+} ions of the Cu_3O trimers as compared to the Cu^{2+} ions of the copper paddlewheels. Using CMC, a binding energy of roughly 5.0 kJmol^{-1} was calculated for sorption onto the Cu3 ion.

The utilization of many-body polarization interactions in simulation can be a useful tool to identify the different sorption sites in a MOF *via* the distribution of the induced dipoles. Figure 7 shows a plot of the hydrogen dipole magnitudes against the normalized hydrogen population in *rht*-MOF-1 at 77 K and 0.01 atm as well as 1.0 atm. Each region for the induced dipole magnitudes corresponds to a specific site of occupancy inside the MOF. For *rht*-MOF-1, three different regions in the dipole distribution can be identified; the ranges are the following: 0.30 D and above, 0.20 D to 0.30 D, and 0.00 D to 0.20 D. The peak from 0.30 D and above corresponds to sorption onto the Cu1 ions of the paddlewheels (Figure 8(a)). This is consistent to what was observed in the dipole distribution for other *rht*-MOFs, as the highest dipole magnitude range correlates to sorption onto the preferred Cu^{2+} ion of the paddlewheel in the MOF.[36,37] A molecular illustration depicting the sorption of a hydrogen molecule onto a Cu1 ion in *rht*-MOF-1 is shown Figure 9(a). The center-of-mass of the sorbed hydrogen molecule is approximately 2.5 Å from the Cu1 ion. Indeed, this site corresponds to the radial distribution peak that was observed about the Cu1 ions at 2.5 Å. Further, the hydrogen molecules sorb about the Cu1 ions in a T-shaped manner, which is consistent to the hydrogen molecule orientation that was observed about the Cu^{2+} ions in HKUST-1 through *ab initio* simulation studies.[44] Note, the peak from 0.30 D and above is smaller at 1.0 atm compared to at 0.01 atm, which indicates that there is less occupancy about the Cu1 ions at higher pressures.

The dipole distribution for *rht*-MOF-1 shows a large peak from 0.20 D to 0.30 D at 0.01 atm. This peak mainly corresponds to the sorption of hydrogen onto the nitrate ions as well as the Cu^{2+} ions of the Cu_3O trimers (Figure 8(b)). In addition, some hydrogen molecules with these dipole magnitudes can be seen sorbing onto the Cu1 ions. A large number of hydrogen molecules with these induced dipoles can be found in the vicinity of the nitrate ions in the corners of the truncated tetrahedral cages at this pressure, which is consistent with the notion that the nitrate ions are highly preferred in this MOF at low loading. Note, the corners of the truncated tetrahedral cages have been observed as a sorption site in other *rht*-MOFs.[36,37] In *rht*-MOF-1, this region is much more favorable at initial loading due to the presence of the unbound nitrate ions in this area. Note, although the nitrate ions provide the greatest binding affinity towards the hydrogen molecules, these counterions induce lower dipoles on the adsorbate molecules than the Cu^{2+} ions of the copper paddlewheels. This is because the D_{3h} symmetry exhibited by the nitrate ions causes the dipole moments to lessen. A few hydrogen molecules can be seen sorbing onto the Cu3 ions at this pressure, although these ions are not as preferred as the nitrate ions and the Cu1 ions at low loading. For sorption onto this site, examination of the system's coordinates revealed that the hydrogen molecules make a T-shaped interaction about the Cu^{2+} ions of the Cu_3O trimers (Figure 9(b)). This interaction is similar to what was observed for the hydrogen molecule orientation about the Cu^{2+} ions of the paddlewheels. For the Cu3 ion, the distance between the center-of-mass of the sorbed hydrogen molecule and the Cu^{2+} ion is approximately 2.7 Å, which is consistent with

Journal of Materials Chemistry A Accepted Manuscript

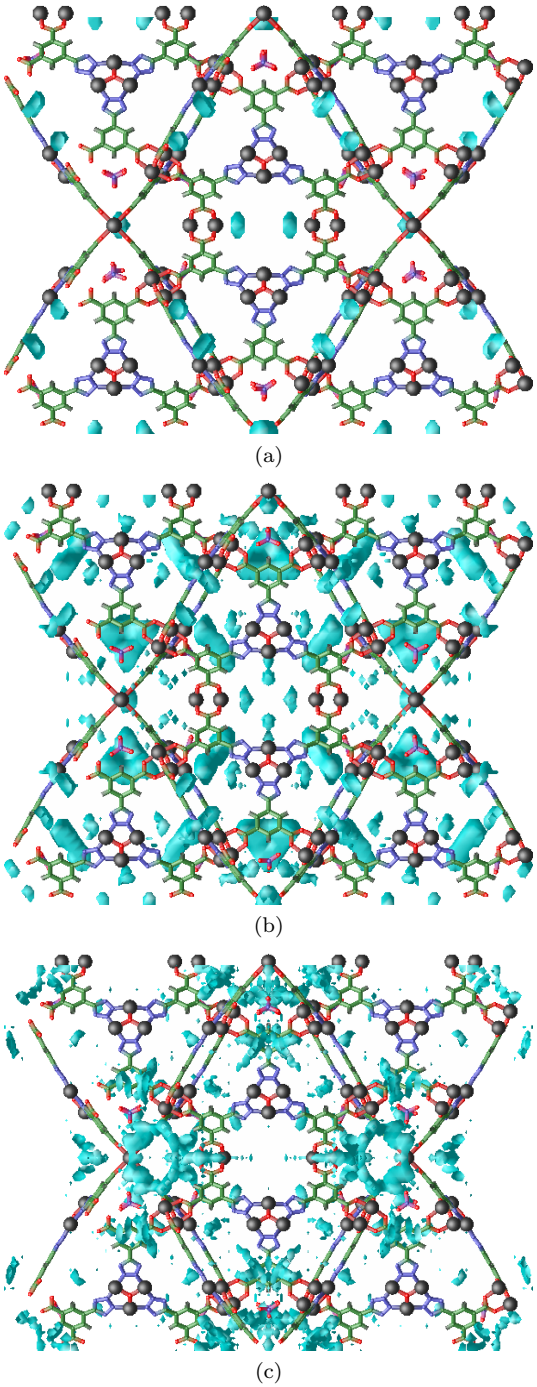

FIG. 8: The three–dimensional histograms in *rht*-MOF-1 showing the sites of hydrogen sorption (cyan) as a function of induced dipole magnitude according to Figure 7: **(a)** 0.30 Debye and above **(b)** 0.20 to 0.30 Debye **(c)** 0.00 to 0.20 Debye. MOF atom colors: C = green, H = white, N = blue, O = red, Cu = black.

the radial distribution peak observed around this ion at that distance. It can be seen that the peak from 0.20 D to 0.30 D is severely reduced at 1.0 atm. This is because there is less sorption onto the nitrate ions and Cu1 ions at this pressure. Additionally, sorption onto the Cu3 ions becomes more prominent at 1.0 atm.

The population with the lowest induced dipoles in *rht*-MOF-1, ranging from 0.00 D to 0.20 D, corresponds to sorption within the cuboctahedral cages of the MOF (Figure 8(c)). Visual inspection of the modeled system cell revealed that these hydrogen molecules sorb onto the sides of the copper paddlewheels (Figure 10). The occupancy of hydrogen

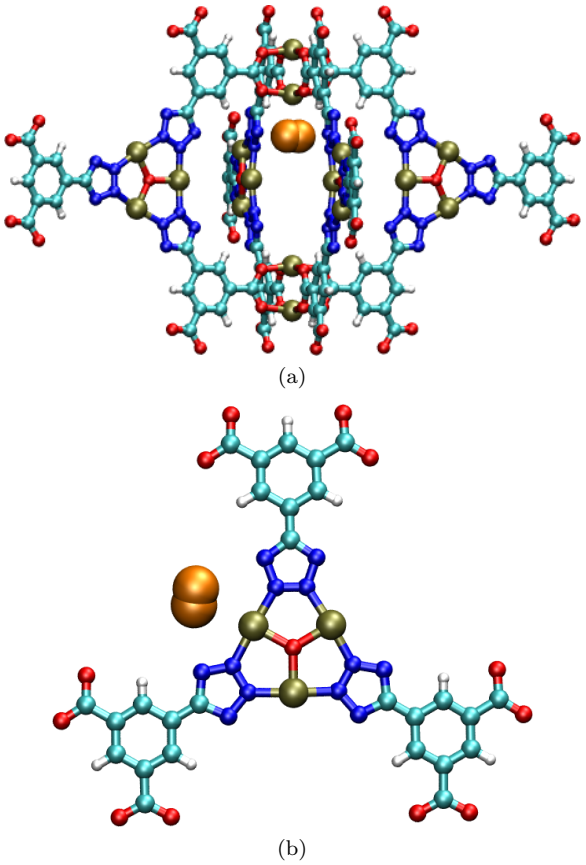

FIG. 9: Molecular illustration of the hydrogen binding site about **(a)** the Cu1 ion and **(b)** the Cu3 ion in *rht*-MOF-1 as determined from simulation. The adsorbate molecules are shown in orange. MOF atom colors: C = cyan, H = white, N = blue, O = red, Cu = tan.

molecules in this cage is low at 0.01 atm. This is because other favorable sites (e.g., the nitrate ions, the Cu1 ions, the Cu3 ions) are being occupied first at this loading. However, at 1.0 atm, the peak from 0.00 D to 0.20 D increases, which signifies that this area of the MOF becomes more populated at higher pressures. As the more favorable sorption sites become filled, the hydrogen molecules will essentially crowd into other areas of the MOF; in the case of *rht*-MOF-1, the regions are the cuboctahedral cages where the hydrogen molecules can sorb onto the sides of the paddlewheels.

In order to confirm that the aforementioned sites are indeed the proper binding sites for hydrogen in *rht*-MOF-1, the two-dimensional quantum rotational levels for a hydrogen molecule about each site were calculated (Table I); these levels were compared to the transitions that are observed in the experimental INS spectra for hydrogen in *rht*-MOF-1. Note, in vacuum, the rotational energy levels for a hydrogen molecule are characteristic of a rigid rotor. However, in the presence of an external field (e.g., a MOF sorption site), the energy levels for the hydrogen molecule split since the field breaks the degeneracy. The INS spectra for hydrogen in *rht*-MOF-1 is shown in Figure 11 for two different loadings. The calculation of the rotational energy levels for a hydrogen molecule sorbed in the proximity of a nitrate ion located in the corner of the truncated tetrahedral cage (site 1) revealed a value of 5.63 meV for the $j = 0$ to $j = 1$ transition. Evaluation of the INS spectra revealed a small, but noticeable peak at approximately 5 meV for both loadings. This peak must correspond to the sorption of hydrogen onto

Journal of Materials Chemistry A Accepted Manuscript

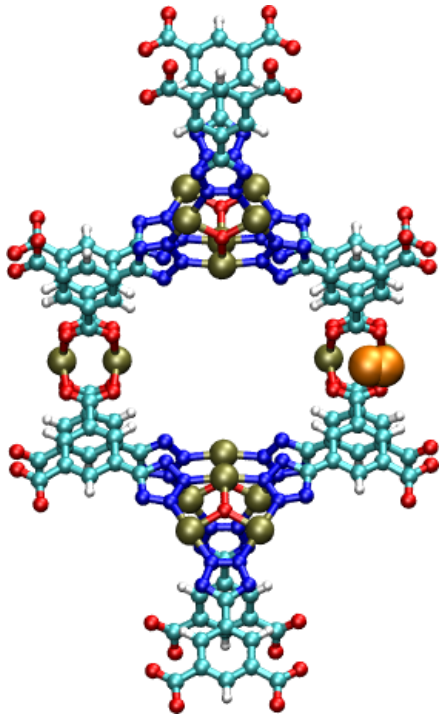

FIG. 10: Molecular illustration of the hydrogen binding site about the sides of the copper paddlewheels within the cuboctahedral cage in *rht*-MOF-1 as determined from simulation. The adsorbate molecule is shown in orange. MOF atom colors: C = cyan, H = white, N = blue, O = red, Cu = tan.

the nitrate ions in *rht*-MOF-1. The nitrate ions are the most favorable sites for hydrogen sorption in the MOF and there is a strong interaction between these ions and the hydrogen molecules. Therefore, it makes sense that this interaction would be found at lower energies in the INS spectra.

Note, it seems that the presence of the nitrate ions in *rht*-MOF-1 causes most of the INS spectra to become very broad. A similar finding was observed in the INS spectra for In-*soc*-MOF.[92] Moreover, it is expected that the peak at approximately 5 meV should be more pronounced in the INS spectra for *rht*-MOF-1. It is hypothesized that the presence of the nitrate ions in the framework would make it difficult to fully activate the material. As a result, it is possible that there are solvent molecules occupying the corners of the truncated tetrahedral cages when the INS studies were performed. Small amounts of solvent have a much more pronouced effect on the INS spectra than on the sorption measurements.

The rotational energy level for a hydrogen molecule sorbed onto the Cu1 ions in a T-shaped configuration (site 2) was calculated to be 9.72 meV for the lowest transition. This value is in good agreement to the transition that is observed at approximately 9 meV in the INS spectra. The INS spectra for hydrogen in other MOFs containing copper paddlewheels, such as HKUST-1,[44,91] PCN-12,[93] and *rht*-MOF-4a[25] revealed a peak near 9 meV as well. Thus, this transition must be associated with sorption onto the Cu^{2+} ions of the paddlewheels as verified through the calculations performed herein and in previous work.[44] This is consistent with a previously mentioned hypothesis that a peak located in the range of 7 to 10 meV in the INS spectra for a MOF containing copper paddlehweels corresponds to a hydrogen molecule interacting with a single open-metal Cu^{2+} ion site for the lowest rotational tunneling transition.[93] Note, the two lowest transitions for site 2 in *rht*-MOF-1 (calculated to be 9.72 and 10.81 meV, respectively) are fairly well defined at the higher loading.

n	j	Site 1 ΔE (meV)	Site 2 ΔE (meV)	Site 3 ΔE (meV)	Site 4 ΔE (meV)
1	0	0.00	0.00	0.00	0.00
2		5.63	9.72	6.92	14.02
3	1	23.11	10.81	15.70	14.70
4		24.76	34.98	32.53	15.44
5		42.73	35.36	38.62	43.10
6		43.46	56.99	39.46	44.04
7	2	43.70	70.60	50.60	44.10
8		56.73	71.70	57.14	44.23
9		56.84	75.93	63.91	45.30

TABLE I: The calculated two-dimensional quantum rotational levels (in meV) for a hydrogen molecule at different sites in *rht*-MOF-1. Sites 1, 2, 3, and 4 are depicted in Figures 5, 9(a), 9(b), and 10, respectively. The energies are given relative to E_0, which are -86.17 meV, -71.93 meV, -38.09 meV, and -44.06 meV for the respective sites.

For a hydrogen molecule sorbed onto the Cu3 ions of the Cu_3O trimers (site 3), a rotational level of 6.92 meV was calculated for the lowest transition. It can be seen in the INS spectra that a broad peak spans the region from approximately 6.5 to 8.0 meV. In addition, this peak is more noticeable at the higher loading. Because this peak seems to get larger at higher loadings and since the Cu3 ions are occupied at higher pressures, especially after the Cu1 ions are populated, this region in the INS spectra must be associated with sorption onto the Cu3 ions. This is consistent to what was observed in the simulations and the calculations for a hydrogen molecule about this site. It is interesting to note that sorption onto the Cu^{2+} ions that are part of the Cu_3O trimer has a lower energy (higher barrier to rotation) than sorption onto the Cu^{2+} ions of copper paddlewheels even though the former gets occupied only at higher loadings. This could be due to the fact that the Cu3 ions are more easily accessible in the framework than the Cu1 ions. However, the higher electron density (lower positive charge) of the Cu3 ions relative to the Cu1 ions causes the latter to become more preferred at low loadings.

The INS spectra for hydrogen in *rht*-MOF-1 shows a large peak at about 14 meV. The simulations revealed that the adsorbate molecules can occupy the cuboctahedral cages (site 4) at higher loadings after sites 1, 2, and 3 are filled. This site was observed in the dipole distribution for the polarizable hydrogen potential in the MOF. The quantum rotation calculations revealed that this site indeed corresponds to the peak at approximately 14 meV. This is a weak site for hydrogen sorption in the MOF, and as a consequence, the rotational tunneling transition for this site is found at higher energies. Moreover, it can be seen that the hydrogen molecules are nearly characteristic of a rigid rotor as they are sorbed within the cavity of the cuboctahedral cage. This is because there is no field acting on the hydrogen molecules as they are sorbed in this region. Indeed, one of the three $j = 1$ sublevels and one of the five $j = 2$ sublevels are exactly the energy of the $j = 1$ and $j = 2$ rigid rotor levels for a hydrogen molecule in the gas phase, respectively (14.70 meV, 44.10 meV). Note, it would be desirable to calculate the entire potential energy surface about each hydrogen sorption site in *rht*-MOF-1 to gain information on the barrier heights for the respective sites. However, the large size of *rht*-MOF-1 unit cell as well as the computational expense of solving the many-body polarization equations makes the calculation rather prohibitive.

Journal of Materials Chemistry A Accepted Manuscript

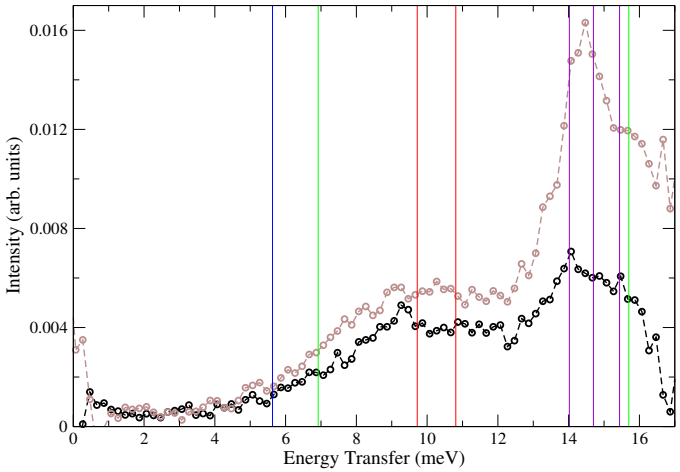

FIG. 11: Inelastic neutron scattering (INS) spectra for hydrogen in *rht*-MOF-1 at different loadings: 1 H_2/Cu (black), and 2 H_2/Cu (pink). The calculated transitions for the different sites as shown in Table I are depicted as vertical colored lines: site 1 = blue, site 2 = red, site 3 = green, site 4 = violet.

IV. CONCLUSION

In conclusion, this work demonstrated the importance of many-body polarization interactions for the simulations of hydrogen sorption in *rht*-MOF-1. Specifically, the inclusion of such interactions was necessary for obtaining outstanding agreement with experimental results and assisting in the identification of the hydrogen binding sites in the MOF. Analysis of the three-dimensional histogram showing the sites of hydrogen sorption for the polarizable hydrogen potential used in *rht*-MOF-1 revealed four distinct sorption sites: the nitrate ions located in the corners of the truncated tetrahedral cages, the Cu1 ions of the copper paddlewheels, the Cu3 ions of the Cu_3O trimers, and the sides of the copper paddlewheels in the cuboctahedral cages.

The calculation of the two-dimensional quantum rotational levels for hydrogen about various moieties in *rht*-MOF-1 confirmed that the considered sites were indeed the likely binding sites for hydrogen sorption in this MOF. The calculated rotational transitions reported in this work were in good agreement with the transitions that were observed experimentally through INS studies. As a result, we were able to associate the different binding sites with certain transitions within the INS spectra for *rht*-MOF-1 and therefore, make a thorough interpretation of the spectra.

It was discovered through the simulation studies that the uncoordinated nitrate ions are more favorable for hydrogen sorption than the open-metal sites at low loading. Sorption onto the nitrate ions corresponds to the high initial Q_{st} value for hydrogen in *rht*-MOF-1, which is 9.5 kJmol^{-1} as determined experimentally. This hydrogen Q_{st} value is considerably higher than those MOFs that contain the copper paddlewheel units, such as HKUST-1.[86] The calculated rotational level for the $j = 0$ to $j = 1$ transition for a hydrogen molecule about the nitrate ions in *rht*-MOF-1 revealed a low energy (high barrier) transition (*ca.* 5 meV), thus indicating a very strong interaction between the hydrogen molecule and the nitrate ions.

For sorption onto the open-metal sites in *rht*-MOF-1, the simulations showed that the Cu1 ions are more preferred than the Cu3 ions at low loading. The Cu^{2+} ions of the copper paddlewheels are the second favored sorption site for hydrogen in *rht*-MOF-1, whereas they are the primary sorption site in other MOFs that contain similar copper paddlewheel units, such as HKUST-1,[44,91] PCN-61,[17,36] Cu-TPBTM,[37] *rht*-MOF-4a,[25] and PCN-12.[93] The INS spectra for hydrogen in *rht*-MOF-1 at low loading reveals a peak at approximately 9 meV, which is comparable to the lowest transition calculated for a hydrogen molecule about the Cu1 ions. In addition, as observed in the INS spectra and the GCMC simulations at higher loadings, the Cu3 ions become occupied after the Cu1 ions despite having a higher barrier to rotation (normally implying greater binding energy) for the lowest transition compared to that for sorption about the Cu1 ions.

Note, while it was appropriate to constrain the nitrate ions to be rigid in their equilibrium positions in *rht*-MOF-1 for the simulation conditions considered in this work, this approach would be inefficient for GCMC simulations of other gases, such as CO_2, CH_4, and N_2 at higher temperatures (e.g., 298 K) in this MOF. This is because the nitrate ions are mobile in *rht*-MOF-1 at higher temperatures and they can migrate to other regions in the MOF that can affect overall sorption. This was confirmed by performing MD simulations to investigate the mobility of the nitrate ions in *rht*-MOF-1 at higher temperatures. Note, this phenomenon was demonstrated in previous modeling studies on *rht*-MOF-1 as well.[40] Thus, currently, we cannot perform GCMC simulations of CO_2, CH_4, and N_2 sorption in *rht*-MOF-1 at ambient temperatures with reasonable accuracy without accounting for the mobility of the counterions through the inclusion of dynamics or sampling the positions of the counterions thermally.

Though *rht*-MOF-1 contains two types of open-metal sites and include extra-framework nitrate ions that contributes to a large hydrogen uptake capacity, this MOF exhibits a high surface area and contains pore sizes that are larger than most other MOFs. Thus, while the hydrogen uptake in *rht*-MOF-1 at 77 K and 1.0 atm is remarkably 2.4 wt %, there are other MOFs that have higher hydrogen uptake under the same conditions,[7,94] such as Mg-MOF-74,[95] In-*soc*-MOF,[92] HKUST-1,[86] and PCN-12.[93] It is noteworthy that the aforementioned MOFs have lower surface areas and pore sizes compared to *rht*-MOF-1. In addition, when comparing to other members of the *rht*-MOF platform, *rht*-MOF-1 contains larger truncated octahedral and truncated tetrahedral cages relative to other *rht*-MOFs that display high hydrogen uptake. For instance, hydrogen sorption studies in Cu-TPBTM[37] and Cu-TDPAT,[21] the two smallest members of the *rht*-MOF platform, revealed that these MOFs sorb 2.61 wt % and 2.65 wt % of hydrogen at 77 K and 1.0 atm, respectively. Thus, reducing the pore sizes of the framework seems to be a promising strategy for increasing hydrogen sorption in MOFs, as smaller pores would allow the hydrogen molecules to interact with more atoms of the framework simultaneously.

Overall, the results from this study demonstrate the necessity of incorporating many-body polarization interactions for the simulations of hydrogen sorption in a highly charged/polar MOF, such as *rht*-MOF-1. The correct sorption behavior between the hydrogen molecules and the open-metal sites cannot be captured if this potential energy term is not included in the simulations. Further, the combination of explicit polarization in simulation and quantum rotation calculations assisted in the identification of the binding sites for hydrogen sorption for the MOF investigated herein. This study also demonstrates the power of using careful sim-

Journal of Materials Chemistry A Accepted Manuscript

ulations in conjunction with complementary experiments to form a wholisitic picture of MOFs as gas storage/separation vehicles. Current work is underway to execute similar procedures in other MOFs. In general, GCMC simulations and INS studies can provide detailed insights into the mechanism of hydrogen sorption in a variety of MOFs. The results from these studies can help experimentalists gain new perspectives into creating novel MOFs with improved hydrogen uptake capacity.

ASSOCIATED CONTENT

Supporting Information. Details of molecular dynamics simulations, many-body polarization, grand canonical Monte Carlo methods and electronic structure calculations, tables of properties, and additional content.

AUTHOR INFORMATION

Corresponding Author
*E-mail: brian.b.space@gmail.com
Author Contributions
§Authors contributed equally
Notes
The authors declare no competing financial interest.

ACKNOWLEDGMENTS

This work was supported by the National Science Foundation (Award No. CHE-1152362). Computations were performed under a XSEDE Grant (No. TG-DMR090028) to B.S. This publication is also based on work supported by Award No. FIC/2010/06, made by King Abdullah University of Science and Technology (KAUST). The authors also thank the Space Foundation (Basic and Applied Research) for partial support. The authors would like to acknowledge the use of the services provided by Research Computing at the University of South Florida.

Journal of Materials Chemistry A Accepted Manuscript

[1] Haryanto, A.; Fernando, S.; Murali, N.; Adhikari, S. *Energy & Fuels* **2005**, *19*, 2098–2106.
[2] Belof, J. L.; Stern, A. C.; Eddaoudi, M.; Space, B. *Journal of the American Chemical Society* **2007**, *129*, 15202–15210, PMID: 17999501.
[3] Collins, D. J.; Ma, S.; Zhou, H.-C. In *Metal-Organic Frameworks: Design and Application*; MacGillivray, L. R., Ed.; John Wiley & Sons, Inc.: Hoboken, NJ, 2010; pp 249–266.
[4] DOE Targets for Onboard Hydrogen Storage Systems for Light-Duty Vehicles. 2009; `http://www1.eere.energy.gov/hydrogenandfuelcells/storage/pdfs/targets_onboard_hydro_storage.pdf`.
[5] Collins, D. J.; Zhou, H.-C. *J. Mater. Chem.* **2007**, *17*, 3154–3160.
[6] Zhao, D.; Yuan, D.; Zhou, H.-C. *Energy Environ. Sci.* **2008**, *1*, 222–235.
[7] Suh, M. P.; Park, H. J.; Prasad, T. K.; Lim, D.-W. *Chemical Reviews* **2012**, *112*, 782–835.
[8] Yaghi, O. M.; Li, H.; Davis, C.; Richardson, D.; Groy, T. L. *Accounts of Chemical Research* **1998**, *31*, 474–484.
[9] Hynek, S.; Fuller, W.; Bentley, J. *International Journal of Hydrogen Energy* **1997**, *22*, 601 – 610.
[10] Nijkamp, M.; Raaymakers, J.; van Dillen, A.; de Jong, K. *Applied Physics A* **2001**, *72*, 619–623.
[11] Sakintuna, B.; Lamari-Darkrim, F.; Hirscher, M. *International Journal of Hydrogen Energy* **2007**, *32*, 1121 – 1140.
[12] Eddaoudi, M.; Moler, D. B.; Li, H.; Chen, B.; Reineke, T. M.; O'Keeffe, M.; Yaghi, O. M. *Accounts of Chemical Research* **2001**, *34*, 319–330, PMID: 11308306.
[13] Eddaoudi, M.; Eubank, J. F. In *Metal-Organic Frameworks: Design and Application*; MacGillivray, L. R., Ed.; John Wiley & Sons, Inc.: Hoboken, NJ, 2010; pp 37–89.
[14] Nouar, F.; Eubank, J. F.; Bousquet, T.; Wojtas, L.; Zaworotko, M. J.; Eddaoudi, M. *Journal of the American Chemical Society* **2008**, *130*, 1833–1835.
[15] Zou, Y.; Park, M.; Hong, S.; Lah, M. S. *Chem. Commun.* **2008**, 2340–2342.
[16] Zhao, D.; Yuan, D.; Sun, D.; Zhou, H.-C. *Journal of the American Chemical Society* **2009**, *131*, 9186–9188, PMID: 19530682.
[17] Yuan, D.; Zhao, D.; Sun, D.; Zhou, H.-C. *Angewandte Chemie* **2010**, *122*, 5485–5489.
[18] Farha, O. K.; Yazaydin, A. O.; Eryazici, I.; Malliakas, C. D.; Hauser, B. G.; Kanatzidis, M. G.; Nguyen, S. T.; Snurr, R. Q.; Hupp, J. T. *Nature Chemistry* **2010**, *2*, 944–948.
[19] Zheng, B.; Bai, J.; Duan, J.; Wojtas, L.; Zaworotko, M. J. *Journal of the American Chemical Society* **2011**, *133*, 748–751.
[20] Yan, Y.; Yang, S.; Blake, A. J.; Lewis, W.; Poirier, E.; Barnett, S. A.; Champness, N. R.; Schroder, M. *Chem. Commun.* **2011**, *47*, 9995–9997.
[21] Li, B. et al. *Angewandte Chemie International Edition* **2012**, *51*, 1412–1415.
[22] Eryazici, I.; Farha, O. K.; Hauser, B. G.; Yazaydin, A. O.; Sarjeant, A. A.; Nguyen, S. T.; Hupp, J. T. *Crystal Growth & Design* **2012**, *12*, 1075–1080.
[23] Zheng, B.; Yang, Z.; Bai, J.; Li, Y.; Li, S. *Chem. Commun.* **2012**, *48*, 7025–7027.
[24] Luebke, R.; Eubank, J. F.; Cairns, A. J.; Belmabkhout, Y.; Wojtas, L.; Eddaoudi, M. *Chem. Commun.* **2012**, *48*, 1455–1457.
[25] Eubank, J. F.; Nouar, F.; Luebke, R.; Cairns, A. J.; Wojtas, L.; Alkordi, M.; Bousquet, T.; Hight, M. R.; Eckert, J.; Embs, J. P.; Georgiev, P. A.; Eddaoudi, M. *Angewandte Chemie International Edition* **2012**, *51*, 10099–10103.
[26] Farha, O. K.; Wilmer, C. E.; Eryazici, I.; Hauser, B. G.; Parilla, P. A.; ONeill, K.; Sarjeant, A. A.; Nguyen, S. T.; Snurr, R. Q.; Hupp, J. T. *Journal of the American Chemical Society* **2012**, *134*, 9860–9863.
[27] Farha, O. K.; Eryazici, I.; Jeong, N. C.; Hauser, B. G.; Wilmer, C. E.; Sarjeant, A. A.; Snurr, R. Q.; Nguyen, S. T.; Yazaydn, A. .; Hupp, J. T. *Journal of the American Chemical Society* **2012**, *134*, 15016–15021.
[28] Zhao, X.; Sun, D.; Yuan, S.; Feng, S.; Cao, R.; Yuan, D.; Wang, S.; Dou, J.; Sun, D. *Inorganic Chemistry* **2012**, *51*, 10350–10355.
[29] Wang, X.-J.; Li, P.-Z.; Chen, Y.; Zhang, Q.; Zhang, H.; Chan, X. X.; Ganguly, R.; Li, Y.; Jiang, J.; Zhao, Y. *Scientific Reports* **2013**, *3*, DOI:10.1038/srep01149.
[30] Wilmer, C. E.; Farha, O. K.; Yildirim, T.; Eryazici, I.; Krungleviciute, V.; Sarjeant, A. A.; Snurr, R. Q.; Hupp, J. T. *Energy Environ. Sci.* **2013**, *6*, 1158–1163.
[31] Yan, Y.; Suyetin, M.; Bichoutskaia, E.; Blake, A. J.; Allan, D. R.; Barnett, S. A.; Schröder, M. *Chemical Science* **2013**, *4*, 1731–1736.
[32] Bhatia, S. K.; Myers, A. L. *Langmuir* **2006**, *22*, 1688–1700.
[33] Ma, S. *Pure and Applied Chemistry* **2009**, *81*, 2235–2251.
[34] Yang, Q.; Zhong, C. *The Journal of Physical Chemistry B* **2006**, *110*, 17776–17783.
[35] Rosi, N. L.; Eckert, J.; Eddaoudi, M.; Vodak, D. T.; Kim, J.; O'Keeffe, M.; Yaghi, O. M. *Science* **2003**, *300*, 1127–1129.
[36] Forrest, K. A.; Pham, T.; McLaughlin, K.; Belof, J. L.; Stern, A. C.; Zaworotko, M. J.; Space, B. *The Journal of Physical Chemistry C* **2012**, *116*, 15538–15549.
[37] Pham, T.; Forrest, K. A.; Nugent, P.; Belmabkhout, Y.; Luebke, R.; Eddaoudi, M.; Zaworotko, M. J.; Space, B. *The Journal of Physical Chemistry C* **2013**, *117*, 9340–9354.
[38] Cirera, J.; Sung, J. C.; Howland, P. B.; Paesani, F. *J. Chem. Phys.* **2012**, *137*, 054704.
[39] Paesani, F. *Molecular Simulation* **2012**, *38*, 631–641.
[40] Babarao, R.; Eddaoudi, M.; Jiang, J. W. *Langmuir* **2010**, *26*, 11196–11203.
[41] Cai, J.; Xing, Y.; Zhao, X. *RSC Advances* **2012**, *2*, 8579–8586.
[42] Yang, Q.; Liu, D.; Zhong, C.; Li, J.-R. *Chemical Reviews* **2013**, *113*, 8261–8323.
[43] Feynman, R. P.; Hibbs, A. R. *Quantum Mechanics and Path Integrals*; McGraw-Hill: New York, 1965; Chapt. 10, Sect. 3, pg. 281.
[44] Brown, C. M.; Liu, Y.; Yildirim, T.; Peterson, V. K.; Kepert, C. J. *Nanotechnology* **2009**, *20*, 204025.
[45] Matanović, I.; Belof, J. L.; Space, B.; Sillar, K.; Sauer, J.; Eckert, J.; Bačić, Z. *The Journal of Chemical Physics* **2012**, *137*, 014701.
[46] Kong, L.; Román-Pérez, G.; Soler, J. M.; Langreth, D. C. *Physical review letters* **2009**, *103*, 096103.
[47] Kong, L.; Chabal, Y. J.; Langreth, D. C. *Physical Review B* **2011**, *83*, 121402.
[48] Rappé, A. K.; Casewit, C. J.; Colwell, K. S.; Goddard, W. A.; Skiff, W. M. *Journal of the American Chemical Society* **1992**, *114*, 10024–10035.
[49] Kawakami, T.; Takamizawa, S.; Kitagawa, Y.; Maruta, T.; Mori, W.; Yamaguchi, K. *Polyhedron* **2001**, *20*, 1197 – 1206.
[50] Sagara, T.; Klassen, J.; Ganz, E. *J. Chem. Phys.* **2004**, *121*, 12543.
[51] Garberoglio, G.; Skoulidas, A. I.; Johnson, J. K. *The Journal of Physical Chemistry B* **2005**, *109*, 13094–13103, PMID: 16852629.
[52] Yang, Q.; Zhong, C.; Chen, J.-F. *The Journal of Physical Chemistry C* **2008**, *112*, 1562–1569.
[53] Belof, J. L.; Stern, A. C.; Space, B. *The Journal of Physical Chemistry C* **2009**, *113*, 9316–9320.
[54] Stern, A. C.; Belof, J. L.; Eddaoudi, M.; Space, B. *J. Chem. Phys.* **2012**, *136*, 034705.
[55] Pham, T.; Forrest, K. A.; McLaughlin, K.; Tudor, B.; Nugent, P.; Hogan, A.; Mullen, A.; Cioce, C. R.; Zaworotko, M. J.; Space, B. *The Journal of Physical Chemistry C* **2013**, *117*, 9970–9982.
[56] Forrest, K. A.; Pham, T.; Hogan, A.; McLaughlin, K.; Tu-

Journal of Materials Chemistry A Accepted Manuscript

dor, B.; Nugent, P.; Burd, S. D.; Mullen, A.; Cioce, C. R.; Wojtas, L.; Zaworotko, M. J.; Space, B. *The Journal of Physical Chemistry C* **2013**, *117*, 17687–17698.

[57] Forrest, K. A.; Pham, T.; Nugent, P.; Burd, S. D.; Mullen, A.; Wojtas, L.; Zaworotko, M. J.; Space, B. *Crystal Growth & Design* **2013**, *13*, 4542–4548.

[58] van Duijnen, P. T.; Swart, M. *The Journal of Physical Chemistry A* **1998**, *102*, 2399–2407.

[59] Belof, J. L.; Stern, A. C.; Space, B. *Journal of Chemical Theory and Computation* **2008**, *4*, 1332–1337.

[60] Ewald, P. P. *Annalen der Physik* **1921**, *369*, 253–287.

[61] Applequist, J.; Carl, J. R.; Fung, K.-K. *Journal of the American Chemical Society* **1972**, *94*, 2952–2960.

[62] Thole, B. *Chemical Physics* **1981**, *59*, 341 – 350.

[63] Bode, K. A.; Applequist, J. *The Journal of Physical Chemistry* **1996**, *100*, 17820–17824.

[64] McLaughlin, K.; Cioce, C. R.; Pham, T.; Belof, J. L.; Space, B. *The Journal of Chemical Physics* **2013**, *139*, 184112.

[65] Bigeleisen, J.; Mayer, M. G. *The Journal of Chemical Physics* **1947**, *15*, 261.

[66] Abramowitz, M. *Handbook of Mathematical Functions with Formulas, Graphs, and Mathematical Tables* Chapt. 25, Sect. 4, pg. 887.

[67] Belof, J. L. Theory and simulation of metal-organic materials and biomolecules. Ph.D. thesis, University of South Florida, 2009.

[68] Anderson, E.; Bai, Z.; Dongarra, J.; Greenbaum, A.; McKenney, A.; Du Croz, J.; Hammerling, S.; Demmel, J.; Bischof, C.; Sorensen, D. LAPACK: A portable linear algebra library for high-performance computers. Proceedings of the 1990 ACM/IEEE conference on Supercomputing. 1990; pp 2–11.

[69] Belof, J. L.; Space, B. Massively Parallel Monte Carlo (MPMC). Available on Google Code, 2012.

[70] Buch, V. *The Journal of Chemical Physics* **1994**, *100*, 7610.

[71] Darkrim, F.; Levesque, D. *The Journal of Chemical Physics* **1998**, *109*, 4981.

[72] Nicholson, D.; Parsonage, N. G. *Computer Simulation and the Statistical Mechanics of Adsorption*; Academic Press: London, 1982.

[73] Pan, H.; Ritter, J. A.; Balbuena, P. B. *Langmuir* **1998**, *14*, 6323–6327.

[74] Valenzano, L.; Civalleri, B.; Chavan, S.; Palomino, G. T.; Areán, C.; Bordiga, S. *The Journal of Physical Chemistry C* **2010**, *114*, 11185–11191.

[75] Sumida, K.; Horike, S.; Kaye, S. S.; Herm, Z. R.; Queen, W. L.; Brown, C. M.; Grandjean, F.; Long, G. J.; Dailly, A.; Long, J. R. *Chemical Science* **2010**, *1*, 184–191.

[76] Dietzel, P. D.; Panella, B.; Hirscher, M.; Blom, R.; Fjellvåg, H. *Chemical Communications* **2006**, 959–961.

[77] Canepa, P.; Nijem, N.; Chabal, Y. J.; Thonhauser, T. *Physical Review Letters* **2013**, *110*, 026102.

[78] Nijem, N.; Canepa, P.; Kong, L.; Wu, H.; Li, J.; Thonhauser, T.; Chabal, Y. J. *Journal of Physics: Condensed Matter* **2012**, *24*, 424203.

[79] Dietzel, P. D.; Johnsen, R. E.; Fjellvåg, H.; Bordiga, S.; Groppo, E.; Chavan, S.; Blom, R. *Chemical Communications* **2008**, 5125–5127.

[80] Canepa, P.; Arter, C. A.; Conwill, E. M.; Johnson, D. H.; Shoemaker, B. A.; Soliman, K. Z.; Thonhauser, T. *J. Mater. Chem. A* **2013**, *1*, 13597–13604.

[81] Lopez, M.; Canepa, P.; Thonhauser, T. *The Journal of Chemical Physics* **2013**, *138*, 154704.

[82] Chui, S. S.-Y.; Lo, S. M.-F.; Charmant, J. P. H.; Orpen, A. G.; Williams, I. D. *Science* **1999**, *283*, 1148–1150.

[83] Lee, J.; Li, J.; Jagiello, J. *Journal of Solid State Chemistry* **2005**, *178*, 2527–2532.

[84] Krawiec, P.; Kramer, M.; Sabo, M.; Kunschke, R.; Fröde, H.; Kaskel, S. *Advanced Engineering Materials* **2006**, *8*, 293–296.

[85] Panella, B.; Hirscher, M.; Pütter, H.; Müller, U. *Advanced Functional Materials* **2006**, *16*, 520–524.

[86] Rowsell, J. L. C.; Yaghi, O. M. *Journal of the American Chemical Society* **2006**, *128*, 1304–1315, PMID: 16433549.

[87] Wong-Foy, A. G.; Matzger, A. J.; Yaghi, O. M. *Journal of the American Chemical Society* **2006**, *128*, 3494–3495.

[88] Xiao, B.; Wheatley, P. S.; Zhao, X.; Fletcher, A. J.; Fox, S.; Rossi, A. G.; Megson, I. L.; Bordiga, S.; Regli, L.; Thomas, K. M.; Morris, R. E. *Journal of the American Chemical Society* **2007**, *129*, 1203–1209, PMID: 17263402.

[89] Chen, B.; Ockwig, N. W.; Millward, A. R.; Contreras, D. S.; Yaghi, O. M. *Angewandte Chemie* **2005**, *117*, 4823–4827.

[90] Nouar, F.; Eckert, J.; Eubank, J. F.; Forster, P.; Eddaoudi, M. *Journal of the American Chemical Society* **2009**, *131*, 2864–2870, PMID: 19206515.

[91] Peterson, V. K.; Liu, Y.; Brown, C. M.; Kepert, C. J. *Journal of the American Chemical Society* **2006**, *128*, 15578–15579.

[92] Liu, Y.; Eubank, J.; Cairns, A.; Eckert, J.; Kravtsov, V.; Luebke, R.; Eddaoudi, M. *Angewandte Chemie International Edition* **2007**, *46*, 3278–3283.

[93] Wang, X.-S.; Ma, S.; Forster, P.; Yuan, D.; Eckert, J.; López, J.; Murphy, B.; Parise, J.; Zhou, H.-C. *Angewandte Chemie International Edition* **2008**, *47*, 7263–7266.

[94] Lässig, D.; Lincke, J.; Moellmer, J.; Reichenbach, C.; Moeller, A.; Gläser, R.; Kalies, G.; Cychosz, K. A.; Thommes, M.; Staudt, R.; Krautscheid, H. *Angewandte Chemie International Edition* **2011**, *50*, 10344–10348.

[95] Dietzel, P. D. C.; Georgiev, P. A.; Eckert, J.; Blom, R.; Strassle, T.; Unruh, T. *Chem. Commun.* **2010**, *46*, 4962–4964.

Journal of Materials Chemistry A Accepted Manuscript

Table of Contents (TOC) Graphic

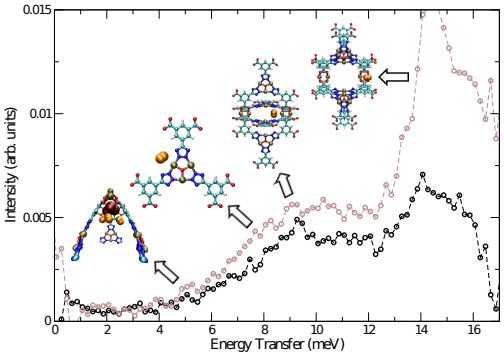

Journal of Materials Chemistry A Accepted Manuscript